Comparison of dynamic effects of high-speed traffic load on ballasted track using a simplified two-dimensional and full three-dimensional model

K Nguyen, JM Goicolea and F Galbadón

Abstract

The vertical dynamic actions transmitted by railway vehicles to the ballasted track infrastructure are evaluated taking into account models with different degrees of detail. In particular, this matter has been studied from a two-dimensional finite-element model to a fully coupled three-dimensional multibody finite-element model. The vehicle and track are coupled via a nonlinear Hertz contact mechanism. The method of Lagrange multipliers is used for the contact constraint enforcement between the wheel and rail. Distributed elevation irregularities are generated based on power spectral density distributions, which are taken into account for the interaction. Due to the contact nonlinearities, the numerical simulations are performed in the time domain, using a direct integration method for the transient problem. The results obtained include contact forces, forces transmitted to the infrastructure (sleeper) by railpads, and envelopes of relevant results for several track irregularities and speed ranges. The main contribution of this work is to identify and discuss coincidences and differences between discrete two-dimensional models and continuum three-dimensional models, as well to assess the validity of evaluating the dynamic loading on the track with simplified two-dimensional models.

Keywords

Dynamic response, infinite element, track irregularities, vehicle–track interaction, wheel–rail contact

Date received: 25 April 2012; accepted: 3 October 2012

Introduction

The advent and success of high-speed railways and the increasing demand for sustainable development is enabling a comeback of railway transport, which is increasing the share in passenger traffic and perhaps also freight traffic. This is a clear trend in Europe and Asia. An implication of this development is the requirement for new standards and regulations, which, among other objectives, must provide criteria for safety and functionality of new or existing railway infrastructure.[1–3]

The evaluation of the dynamic response of railway track subjected to high-speed loading represents one of the main structural issues for the design of high-speed railway structures. The dynamic behaviour of the railway track structure induced by the traffic is influenced by the interaction between the train and the complete track structure, as well as by the dynamic configuration of vehicles. As the operating speed of train becomes higher and reaches 350 km/h or more, accuracy in the analysis of the vehicle–track interaction becomes an important factor to be considered in railway track design. An important number of research works on this subject have contributed to relevant technical advances. Some studies[4–12] have proposed two-dimensional (2D) interaction models in which the vehicle is modelled as one bogie or more realistic models based on rigid bodies connected by suspension systems, and modelling the track as discrete support model. Other detailed models[13–19] were developed to investigate the vertical and lateral dynamic responses of the vehicle–track coupled system in which the vehicle is treated in a more realistic way, and the track is modelled as the three-dimensional (3D) discrete support model or 3D finite-element model. However, these detailed 3D models require large computer resources. Therefore, the optimization of modelling both the rail track and vehicles is an important issue to obtain efficient and reliable models.

This work focuses on issues related to the mechanical actions on the track structure, specifically vertical dynamic loads. The aim of the present work is developing different vehicle–track interaction models, as well as obtaining and comparing the dynamic response on the track structures obtained in these models: the contact force between the wheel and rail, the force transmitted to the railpads, the vibration in the rail, and making recommendations for efficient and rational modelling. For this purpose, a simplified 2D and a full 3D model for the vehicle and track system are formulated by means of the finite-element method, considering the contact between the wheel and rail, vertical track irregularities, for vehicle speed ranges representative of high-speed passenger traffic. The interaction is performed in the time domain using the finite-element software ABAQUS. The results obtained are used to compute the dynamic amplification factor and are further interpreted in the frequency domain. The envelopes of relevant results for several irregularity profiles and speed ranges are obtained and compared between the two models proposed.

Modelling of vehicles

2D model

In the 2D analysis, the vehicle is modelled as a 1/8 railway car (see Figure 1). This model has two vertical degrees of freedom (DOF), in which there are two sprung masses: a mass of 1/8 car body m_c and a mass of 1/4 bogie m_b. The spring and damper elements represent the secondary and primary suspension connecting the car body with the bogie and the bogie with the wheelset, respectively. The wheel is modelled as a mass of 1/2 wheelset m_r, which has contact with the rail. This contact is modelled as a Hertzian spring (details for contact are included in the section on the wheel–rail contact element).

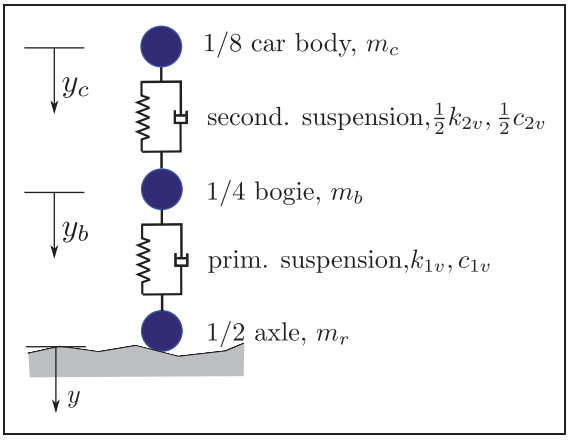

Figure 1. A 1/8 vehicle model.

The equations of motion of the 1/8 vehicle model are written as

$$\begin{cases} m_c\ddot{y}_c + \frac{1}{2}c_{2v}(\dot{y}_c - \dot{y}_b) + \frac{1}{2}k_{2v}(y_c - y_b) = 0 \\ m_b\ddot{y}_b + c_{1v}(\dot{y}_b - \dot{y}_r) + k_{1v}(y_b - y_r) \\ \quad -\frac{1}{2}c_{2v}(\dot{y}_c - \dot{y}_b) - \frac{1}{2}k_{2v}(y_c - y_b) = 0 \end{cases} \quad (1)$$

where k_{2v}, c_{2v}, k_{1v}, c_{1v} are stiffness and damping coefficients of secondary and primary suspension along the Y axis. All parameters used in the simulation can be seen in Appendix 1. Table 1 shows the basic frequencies of vibration of this 2D vehicle model. This characterization considers the wheelset as fixed, i.e. the stiffness of the Hertzian spring for wheel–rail contact is not included.

3D model

In the 3D analysis, some motions as rolling and lateral displacement of vehicle body can be produced by considering the cross-level profiles, which only can be reproduced with a complete 3D vehicle model. Therefore, a complete 3D vehicle model is used in this study for giving more accurate analysis results than using the 2D vehicle model. The vehicle is modelled as a multibody system composed of individual rigid bodies with the mechanical properties corresponding to the high-speed vehicle that are listed in Appendix 1. In order to simplify the analysis, but with enough accuracy, the following assumptions are adopted.

1. The car body, bogies and wheelsets are considered as rigid bodies with associated mass and rotational inertia for each direction (see Figure 2).
2. The car body and the two bogies are connected by the secondary suspension, which is modelled by three linear spring–dashpot elements in the Y axis (k_{2v}, c_{2v}), Z axis (k_{2h}, c_{2h}) and X axis (k_{2l}, c_{2l}).
3. The bogies and wheelsets are connected by the primary suspension, which is represented by three linear spring–dashpot elements. The stiffness and damping coefficients are denoted as k_{1v}, c_{1v} for the Y axis, k_{1h}, c_{1h} for the Z axis and k_{1l}, c_{1l} for the X axis.

Table 1. Frequencies of vibration of the 2D vehicle model.

Vibration modes		
No. of mode	Frequency (Hz)	Description
1	0.79107	Vertical movement of 1/8 car body
2	5.59980	Vertical movement of 1/4 bogie

4. The pitching and yawing motion of the wheelsets are not considered for the purposes of this study.
5. The wheels and rails always keep in contact.

With these assumptions, the car body is described by five DOFs: y_c, z_c, θ_x^c, θ_y^c, θ_z^c, with associated mass M_c and mass moments of inertia J_{cx}, J_{cy}, J_{cz}. The bogie also has five DOFs: y_b, z_b, θ_x^b, θ_y^b, θ_z^b, and the corresponding mass and mass moments of inertia are: M_b, J_{bx}, J_{by}, J_{bz}. For each wheelset, there are three DOFs: y_w, z_w, θ_x^w, the mass M_w and mass moment of inertia J_{wx}. In total, the vehicle model has 27 DOFs.

The vehicle is developed and modelled as a rigid multibody system within the finite-element software ABAQUS. Indeed, the ABAQUS code will solve the full equations, which generate nonlinear and quadratic terms that originate naturally from rigid body dynamics in multibody simulations.[20] Considering our study, which is limited to vertical dynamics, these nonlinear effects are not significant and can be neglected. Therefore, the equations of motion of the vehicle model can be linearized and written in a general form as

$$\mathbf{M}^v\ddot{\mathbf{u}}^v + \mathbf{C}^v\dot{\mathbf{u}}^v + \mathbf{K}^v\mathbf{u}^v = \mathbf{F}^v \tag{2}$$

where $\mathbf{M}^v$, $\mathbf{C}^v$, $\mathbf{K}^v$ are the total mass, damping and stiffness matrices. $\mathbf{u}^v$ is the displacement vector and $\mathbf{F}^v$ is the force vector applied on the vehicle. Some basic frequencies of the 3D model are listed in Table 2 without considering the stiffness of the Hertzian spring for wheel–rail contact (see the section on the wheel–rail contact element). It can be noted that the frequencies of vertical vibration in both the 2D and 3D model are very similar, comparing modes 2 and 7 in Table 2 with those in Table 1.

Modelling of the track

2D model

For modelling the two-dimensional track, several models have been reported in the literature.[6–10,21,22] In general, the rail is modelled as a long beam (Euler or Timoshenko beam formulation) supported on a discrete model of the elastic foundation consisting of railpads, sleepers, ballast, subballast and subgrade.

The track model is discretized with finite elements (see Figure 3). An important feature of this model is that it must have enough length to capture all dynamic effects produced during the vehicle–track interaction. A track length of 90 m has been found sufficient and employed for this study. The rail has been simulated as a continuous Timoshenko beam including shear deformation, supported by pads, which are spring and damper elements. The sleepers are regarded as a concentrated mass. The ballast is

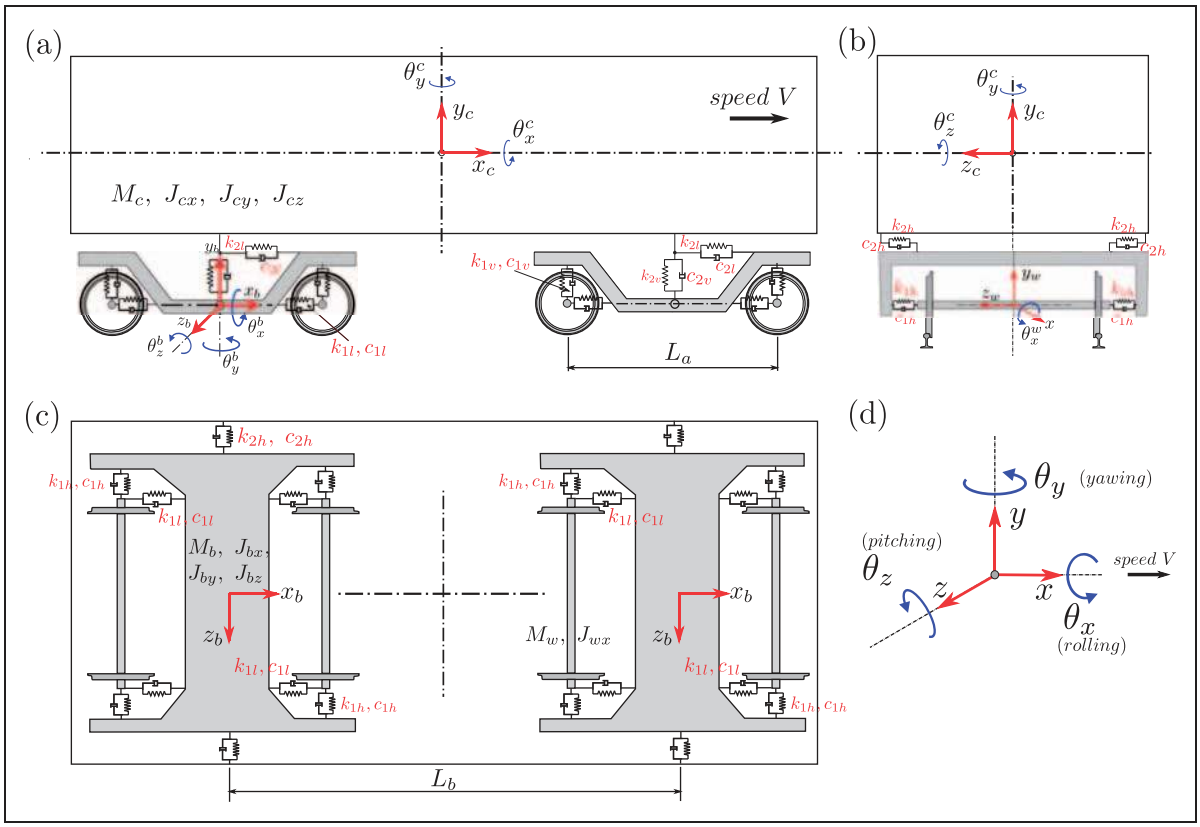

Figure 2. 3D vehicle models: (a) side view; (b) front view; (c) top view; (d) sign convention.

Table 2. Frequencies of vibration of the 3D vehicle model developed in ABAQUS.

Vibration modes		
No. of mode	Frequency (Hz)	Description
1	0.68438	Lateral movement and rolling of car body
2	0.79106	Vertical movement of car body
3	0.87215	Rolling bottom of car body
4	1.22430	Pitching of car body
5	1.37570	Yawing of car body and rolling bogies
7	5.59900	Vertical movement of bogies
9	7.41410	Pitching of bogies
19	23.43000	Yawing of bogies

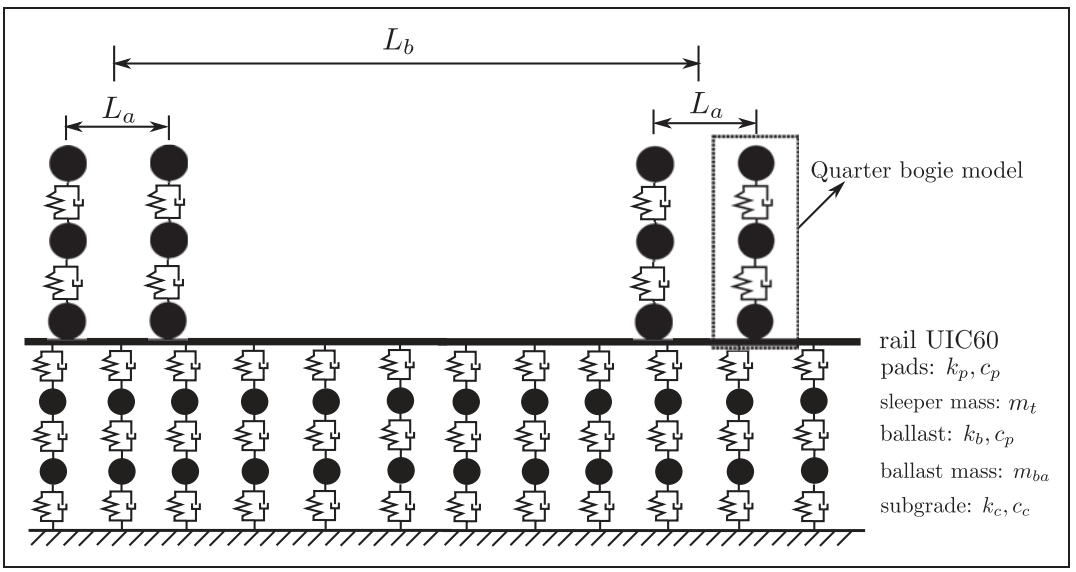

Figure 3. The 2D dynamic model of the vehicle–track system.

represented in a simplified manner by discrete spring and damper elements. The subballast is not considered in this work. The subgrade is modelled as a viscoelastic element without mass. The values of rail-pad stiffness and ballast stiffness are taken from the data of the AVE Zaragoza track.[23] In order to calculate the ballast vibrating mass and the subgrade stiffness, the process proposed by Zhai et al.[24] has been applied, in which the ballast vibrating mass is evaluated as

$$m_{ba} = \rho_b[l_b h_b(l_e + h_b \mathrm{tg}\phi_b) + l_e(h_b^2 - h_0^2)\mathrm{tg}\phi_b + \frac{4}{3}(h_b^3 - h_0^3)\mathrm{tg}^2\phi_b] \quad (3)$$

The subgrade stiffness is calculated by

$$k_c = l_s(l_e + 2h_b \mathrm{tg}\phi_b)E_f \quad (4)$$

where ρ_b is the ballast density, h_b is the depth of ballast, l_e is the effective supporting length of the half sleeper, l_b is the sleeper width underside, ϕ_b is the ballast stress distribution angle, E_f is the elastic modulus of the subgrade and $h_0 = h_b - (l_s - l_b)/(2\mathrm{tg}\phi_b)$ is the height of the overlapping regions.

To determine the damping coefficient of the ballast and the subgrade, the damping coefficients of the ballast and subgrade are assumed as 10% of their critical damping coefficient c_{cr} for independent one DOF systems. With this assumption, the damping coefficients of the ballast and subgrade can be determined by equation (5). All parameters of track used in this study can be seen in Appendix 1.

$$c_b = 0.1 \times 2\sqrt{k_b m_t},\ c_c = 0.1 \times 2\sqrt{k_c m_{ba}} \quad (5)$$

3D model

A 3D finite-element model of the ballast track structure is also considered. The track has the same components and length as the 2D model. The rail is

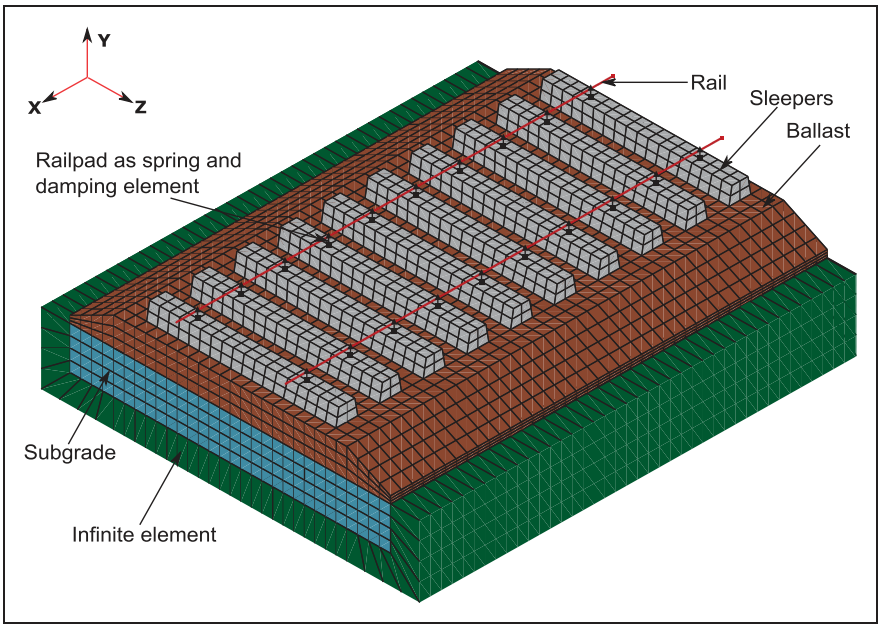

Figure 4. Ballast track model in three dimensions developed in ABAQUS.

modelled as a 3D Timoshenko beam element, resting on discrete supports of railpads. The railpads are modelled as spring and damper elements, which have a vertical stiffness k_p and viscous damping c_p. The sleepers and ballast are modelled as 3D solid elements with the corresponding elastic properties (see Appendix 1). A perfect contact between the sleepers and ballast layer is considered along the track length. Modelling the subgrade is an important issue, as, in principle, a detailed 3D model with standard finite elements should extend to infinity in order to avoid reflection of stress waves transmitted from the structure. Of course, practical considerations make this unfeasible due to excessive computational cost. Among several authors who have studied this problem, Costa[25] performed a comprehensive analysis and concluded that the use of infinite elements was the most precise and effective method. Hence, the infinite elements for the non-reflecting boundaries are used, as implemented in ABAQUS[20] (see Figure 4). These elements are characterized by the fact that an exponentially decay term is multiplied by the shape functions associated with the direction extending to infinity to represent the amplitude attenuation effect of travelling waves. As a result, these elements absorb the energy of waves transmitted from the superstructure of the track, so that no reflections will occur at the boundaries.

The elastic modulus of ballast E_b is adjusted to have the same value of ballast stiffness used in the 2D model. Based on the value of ballast stiffness proposed in the 2D model (k_b), from Zhai et al.[24] the following expression for the elastic modulus of ballast may be obtained

$$E_b = \frac{a_1 + a_2}{a_1 a_2} k_b \tag{6}$$

where $a_1 = 2(l_e - l_b)\mathrm{tg}\phi_b / \ln[(l_e l_s)/(l_b(l_e + l_s - l_b))]$ and $a_2 = l_s(l_s - l_b + 2l_e + 2h_b\mathrm{tg}\phi_b)\mathrm{tg}\phi_b/(l_b - l_s + 2h_b\mathrm{tg}\phi_b)$.

The damping of ballast and subgrade are specified as part of a material definition. For this, ABAQUS provides use of Rayleigh damping.[20] To define this, it is necessary to specify two coefficients: α for mass proportional damping and β for stiffness proportional damping. For each material, ballast and subgrade, the Rayleigh damping factors are determined by[26]

$$\alpha = \xi \frac{2\omega_1\omega_2}{\omega_1 + \omega_2}, \quad \beta = \xi \frac{2}{\omega_1 + \omega_2} \tag{7}$$

The damping ratio ξ is determined as 10% in a frequency range [ω_1, ω_2]. For this study, the frequency range [125, 1885] (rad/s) has been employed, in which the properties of the ballast and subgrade have strong effects on the track dynamics. Accordingly, the value of the Rayleigh damping factors used are: $\alpha = 23.445$ and $\beta = 9.9502 \times 10^{-05}$. The test of decay of motion was taken to verify the correct values of α and β. The mechanical properties of the materials are listed in Appendix 1, and are consistent with the 2D model.

Figure 5 shows the static and dynamic characterization of the track for both the 2D and 3D model. In the static response, a load of 85 kN at the centre point of the rail between two sleepers has been applied for both models. The static track response is very close for both models (see Figure 5a). For obtaining the dynamic track response, a harmonic load is applied at the centre point between two sleepers of the rail, and the amplitudes of displacement and force at the same point are obtained to define the track receptance. For both models, the ballast track has three peaks defining resonances, which

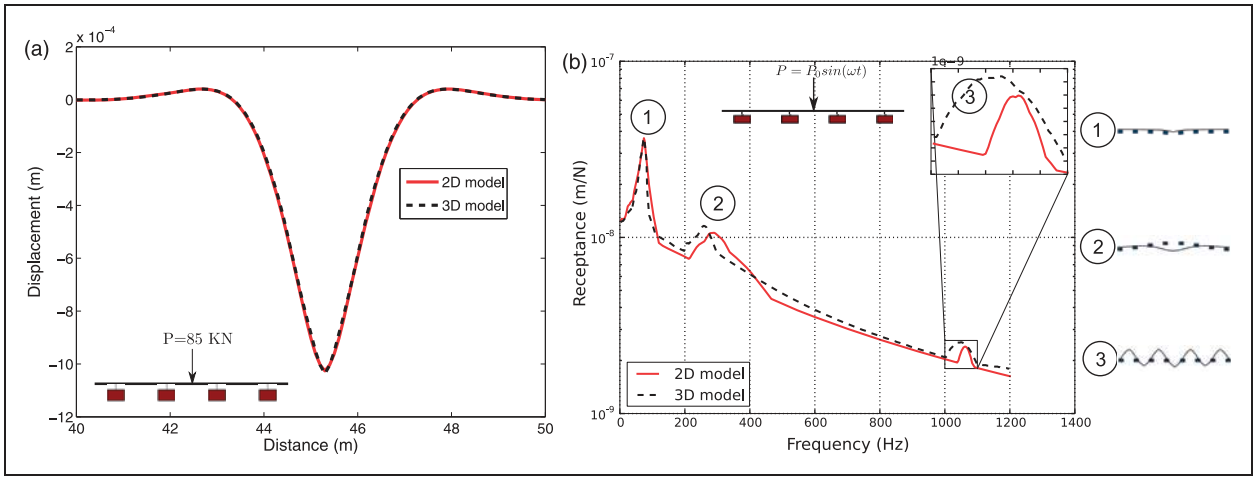

Figure 5. Track response: under (a) static loading and (b) harmonic excitation.

correspond to three fundamental vibration modes (see Figure 5b). The first resonance is due to the vibration of rail-sleepers over the ballast layer (74 Hz for both models). The second peak occurs at 290 Hz for the 2D model and 273 Hz for the 3D model, and is due to the vibration of the rail over the sleepers. And the third peak corresponds to the pin–pin mode, associated with the bending of the rail between the sleeper supports (1065 Hz for the 2D model and 1050 Hz for the 3D model). It can be observed that there is a small difference in amplitude and frequency of the second and third peak between the 2D model and 3D model. The second and third vertical track resonant frequency is clear function of the characteristics of the rail and pads, but also depends on the damping properties, masses of track structure components, etc. In both models, the rail and pads are modelled in the same way, but the other track components of sleepers, ballast and subgrade layer are not. This causes the damping properties and the masses of the track structure components to be not practically the same in both models, which can produce a change in amplitude and frequency of these peaks.[27] In general, the dynamic behaviour of the two models is similar.

Vehicle–track interactions

Generation of track irregularities

Coupling the vehicle system and railway track is realized through interaction forces between the wheels and the rail, where vertical track irregularity profiles (with wavelengths in the range [3–25 m]) is taken into account. The irregularity is generated from the power spectral density (PSD) of the vertical profile and cross level (see Clauss and Schiehlen[28]) according to the maximum considered limit (intervention limit) defined in EN13848-5:2008.[29] The PSD functions used in this study are defined by

$$\Phi_V(\Omega) = A\frac{\Omega_c^2}{(\Omega_r^2+\Omega^2)(\Omega_c^2+\Omega^2)} \tag{8}$$

$$\Phi_C(\Omega) = \frac{A}{l^2}\frac{\Omega_c^2\Omega^2}{(\Omega_r^2+\Omega^2)(\Omega_c^2+\Omega^2)(\Omega_s^2+\Omega^2)}l \tag{9}$$

where $\Phi_V(\Omega)$ is the PSD of the vertical profile, $\Phi_C(\Omega)$ is the PSD of the cross level and Ω is the spatial frequency (rad/m). The values of the constant factors Ω_r, Ω_c, Ω_s, l and A are

$$\Omega_r = 0.0206\,\text{rad/m} \tag{10}$$

$$\Omega_c = 0.8246\,\text{rad/m} \tag{11}$$

$$\Omega_s = 0.4380\,\text{rad/m} \tag{12}$$

$$l = 0.75\,\text{m} \tag{13}$$

$$A = 3.65\times10^{-6}\,(\text{rad m}) \tag{14}$$

For the dynamic analyses, in order to achieve some statistical significance, the three different irregularity profiles have been generated with such limits considering $N = 901$ discrete frequencies. The obtained data are used as input for the the vehicle–track interaction (see Figure 6).

In order to verify the correct generation of track irregularities, the conformity of such profiles is assessed, obtaining the PSD as the Fourier transform of the autocorrelation function of track irregularities generated. Comparisons of the PSD of the generated irregularities profiles and the analytical ones ((8 and 9)) are shown in Figure 7.

Wheel–rail contact elements

During the vehicle/track interaction, the forces are transmitted by means of the wheel–rail contact area.

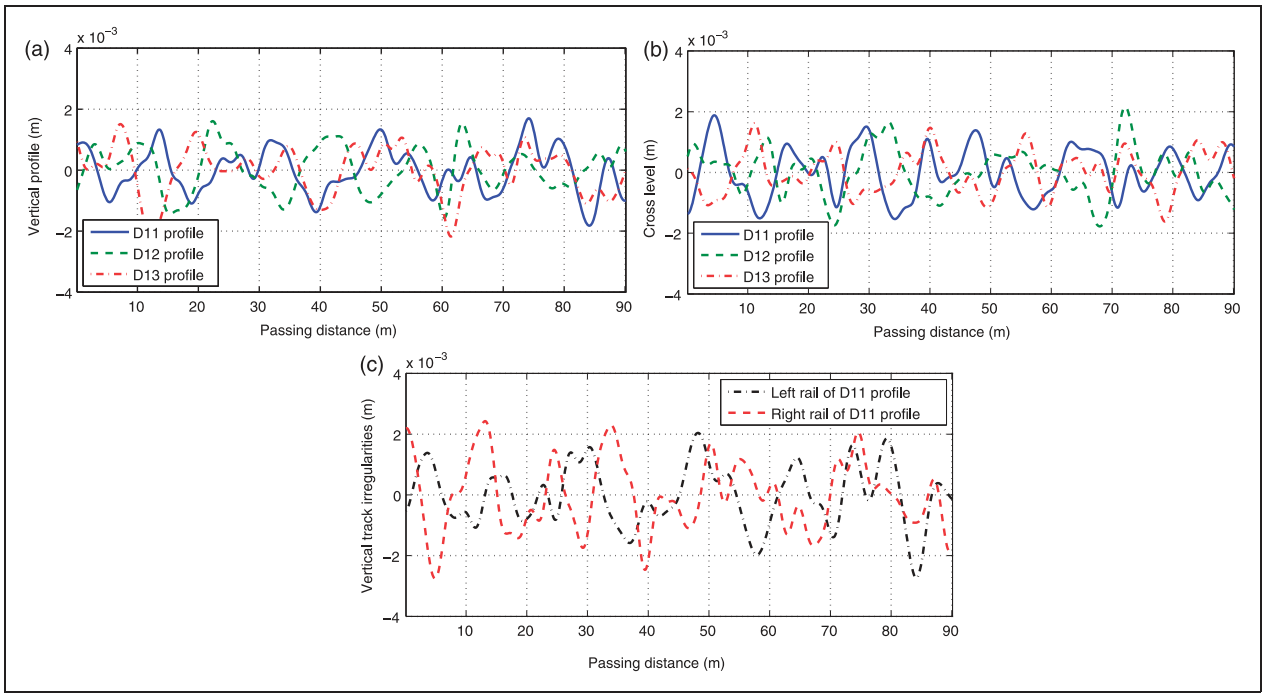

Figure 6. Generation of vertical irregularity profiles: (a) Vertical profiles; (b) Cross levels; (c) Vertical track irregularities.

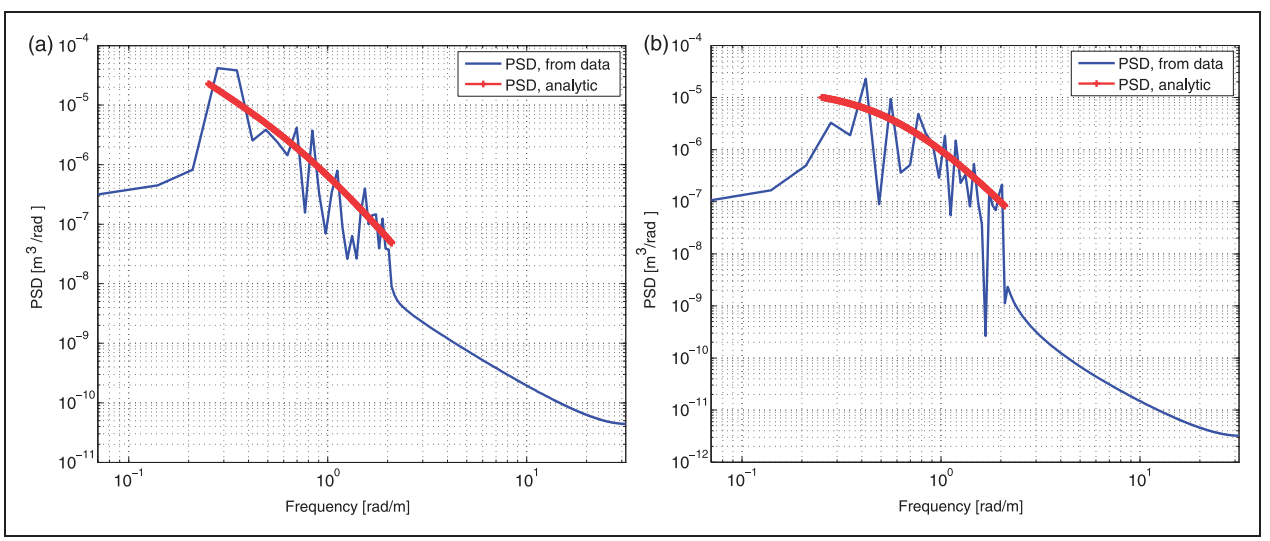

Figure 7. Power spectral densities: (a) Vertical profiles; (b) Cross levels.

On account of the geometry of the contact area between the round wheel and the rail, and under the assumptions that the wheel and rail are the same material with the elastic modulus E and Poisson's ratio ν, using Hertz's normal elastic contact theory,[30] the relationship between the vertical contact force F_v and the vertical relative deformation δ_v is nonlinear and is given by

$$F_v = \delta_v^{3/2} C_H, \text{ where, } C_H = \frac{2E}{3(1-\nu^2)}(r_r r_w)^{1/4} \qquad (15)$$

with r_w the wheel rolling radius and r_r the head radius of the rail cross section. A realistic common case of rail type UIC60 with $E = 2.1 \times 10^{11}\,\mathrm{N/m^2}$, $\nu = 0.3$, $r_r = 0.3\,\mathrm{m}$ and $r_w = 0.455\,\mathrm{m}$ is considered in this study, for which the value of the Hertz coefficient C_H is $9.351 \times 10^{10}\,\mathrm{N/m^{3/2}}$.

The wheel–rail contact is modelled as a Hertzian spring with one node at the centre of the wheel and the other node on the rail, as illustrated in Figure 8. In the literature, the Hertzian spring is often linearized by considering the relationship between the force and the displacement increments from the static wheel load. This assumption is valid when the vertical dynamic contact force does not exceed significantly the vertical static contact force or, in other words,

the vertical relative deformation is not excessive. However, when the rail irregularities exist, the magnitude of the vertical dynamic contact force may be much greater than the static one, and using the linearized Hertzian spring does not lead to the real behaviour of the Hertz contact mechanism. Therefore, in this study the nonlinear behaviour according to equation (15) has been used for the contact.

Simulation results

In order to investigate and compare the 2D and 3D models, some simulations are performed with the models described above, using the finite-element program ABAQUS.[20] For a consistent comparison between the results of the 2D model and 3D model, the uncoupled vehicle composed of four 1/8 vehicle models is used in the 2D simulation (see Figure 3). The calculation is done in the time domain, using the Hilber-Hughes-Taylor (HHT) time integration method to solve the transient problem. In this work, the dynamic effects of high-speed traffic load on the ballasted track are evaluated in a frequency range 0–500 Hz. Consequently, the time step must be small enough to accurately integrate a motion with this frequency range. A constant time step is used and has the value $\Delta t = 0.2 \times 10^{-3}$ s, which satisfies the stability criteria ($\Delta t / T_n \leqslant 0.1$) recommended by Chopra.[26] The Lagrange multiplier method is used for the contact constraint enforcement between the bottom node of the Hertzian spring and the rail surface. The numerical simulations are performed with different speeds (from 200 km/h to 360 km/h) and for each irregularity profile proposed. The following results have been obtained and will be discussed below:

- vertical displacement and acceleration of the bogie;
- contact force between the wheel and the rail;
- force transmitted to the railpads;
- vertical acceleration of the rail;
- envelope of the dynamic amplification factor of the wheel–rail contact force as a function of speed;
- envelope of the dynamic amplification factor of the force transmitted to the railpads.

Figures 9 and 10 show the time history and frequency content (absolute value of the Fourier transform) of vertical displacement and acceleration of the bogie for both models when the train is moving at speed $v = 300$ km/h with track irregularities. From Figure 9, it is noted that in both models, the dominant frequency of vibration is: $f = 4.72$ Hz for the 2D model and $f = 5.55$ Hz for the 3D model. These values are close to the fundamental frequency of vibration of the bogie of 5.6 Hz (Tables 1 and 2), and lie within the frequency of the irregularities, which have a range of [3.33–27.78] Hz for a speed $v = 300$ km/h. From Figure 10, it can be seen that for both models, the frequencies for the acceleration are in the low region (i.e. below 50 Hz); however, the acceleration results for the 2D model show a

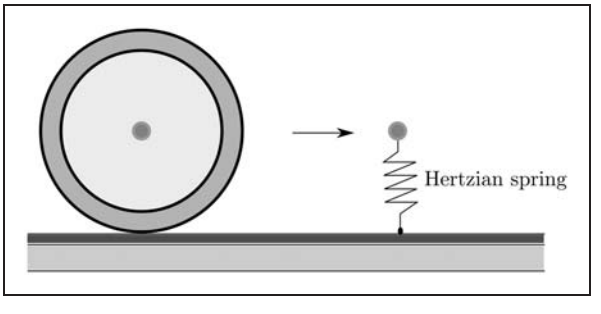

Figure 8. Wheel–rail contact element.

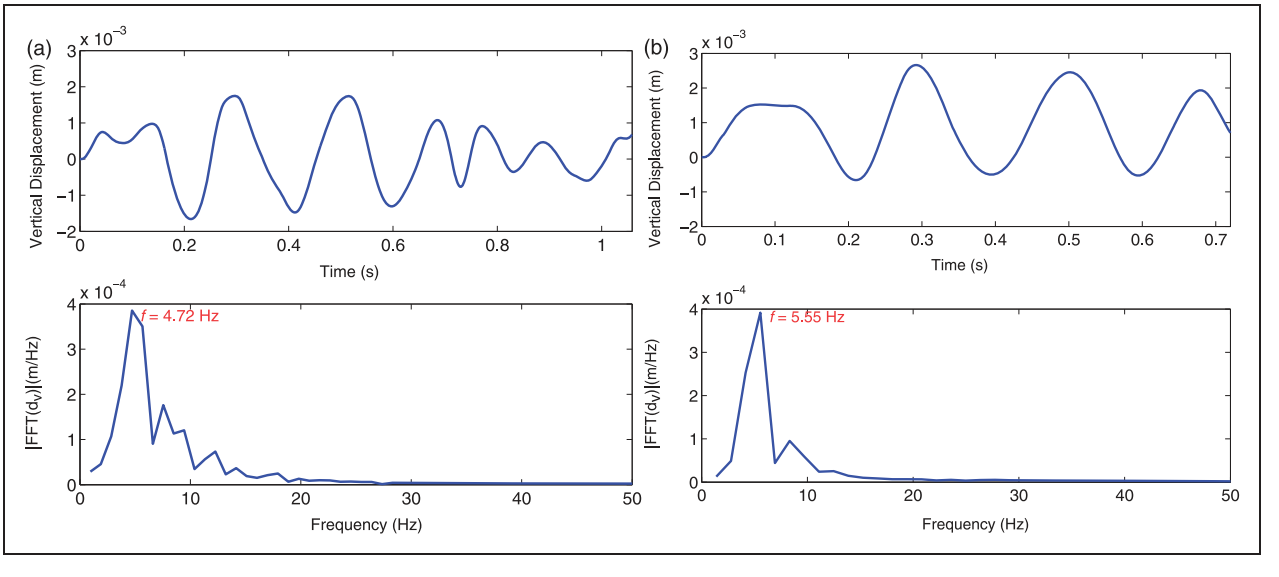

Figure 9. Time history and frequency content of vertical displacement of bogie during the passage of the vehicle on track at speed $v = 300$ km/h with D11 profile: (a) 2D vehicle model result; (b) 3D vehicle model result.

significantly wider band of frequency content than for the 3D model.

Figures 11 and 12 show the results of the contact force between wheel and rail at 340 km/h. Each figure consists of two subfigures, where (a) is the time history and (b) is the frequency content of the dynamic component of contact force.

It can be observed that for both models, the frequency distributions of contact forces consist of a band in a low-frequency range (0–50 Hz) and some isolated resonant frequency peaks for higher frequencies. The lower frequency band is originated by the excitation frequency of the irregularities ([3.78 – 31.48 Hz] for speed $v = 340$ km/h). The resonant peak at approximately 157 Hz is due to the sleeper passage frequency ($f = v/d = 157.4$ Hz for $v = 340$ km/h). This frequency has more influence in the 2D model than in the 3D model.

In Figure 13, a frequency content envelope map for different train speeds is gathered. It can be noted that both models show a frequency response band in the lower frequencies ([0–50] Hz) more or less constant for the entire speed range. This frequency band has higher amplitudes for the 3D model. Additionally, the peaks originated from the sleeper passage are produced at frequencies that increase linearly with speed, as expected. These peaks have greater amplitude for the 2D model. In spite of

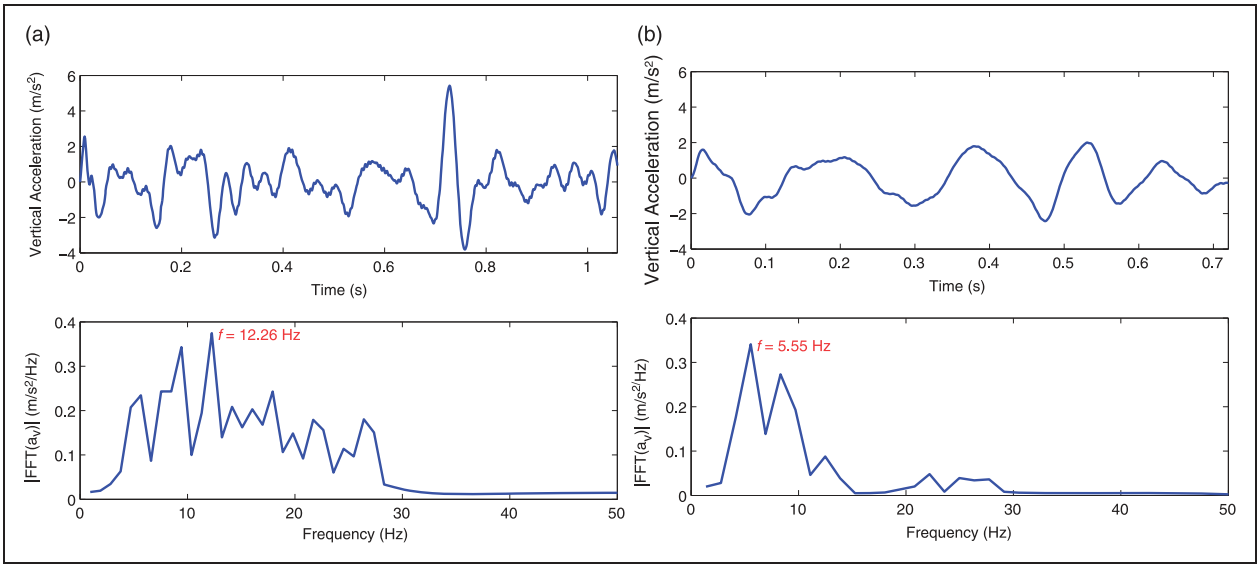

Figure 10. Time history and frequency content of vertical acceleration of bogie during the passage of the vehicle on track at speed $v = 300$ km/h with D11 profile: (a) 2D vehicle model result; (b) 3D vehicle model result.

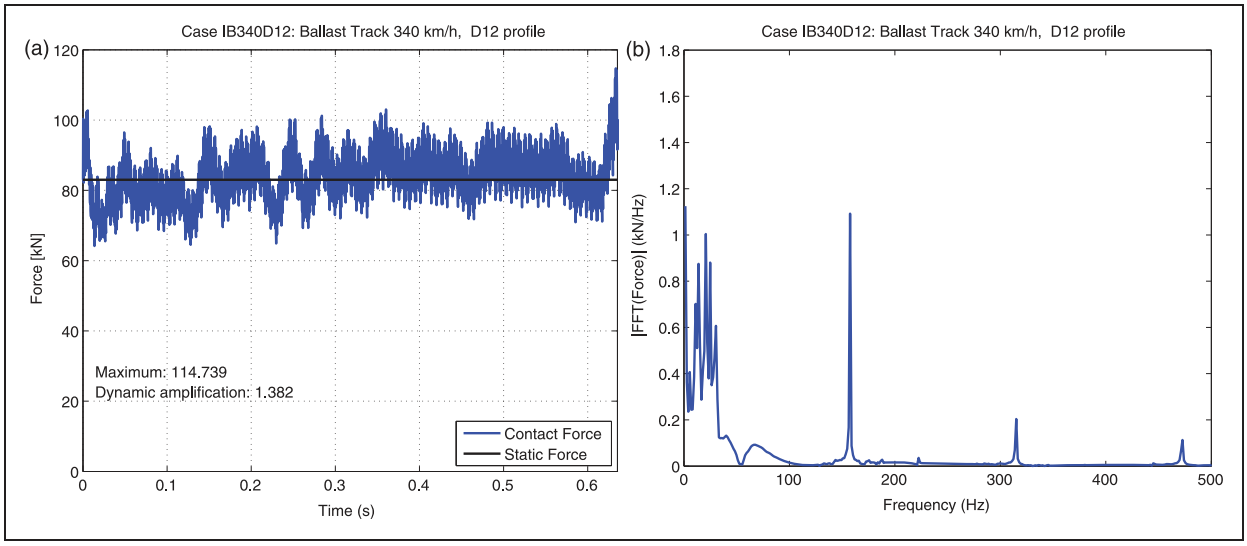

Figure 11. Contact force obtained in 2D model during the passage of vehicle with a speed $v = 340$ km/h: (a) Time history; (b) Frequency content.

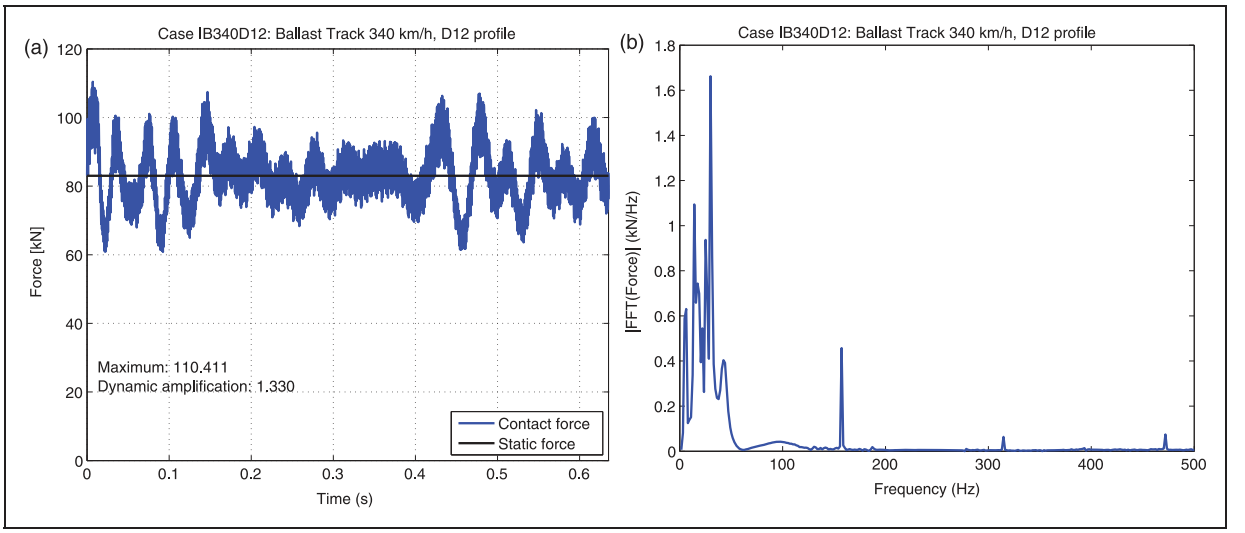

Figure 12. Contact force obtained in 3D model during the passage of vehicle with speed $v = 340$ km/h: (a) Time history; (b) Frequency content.

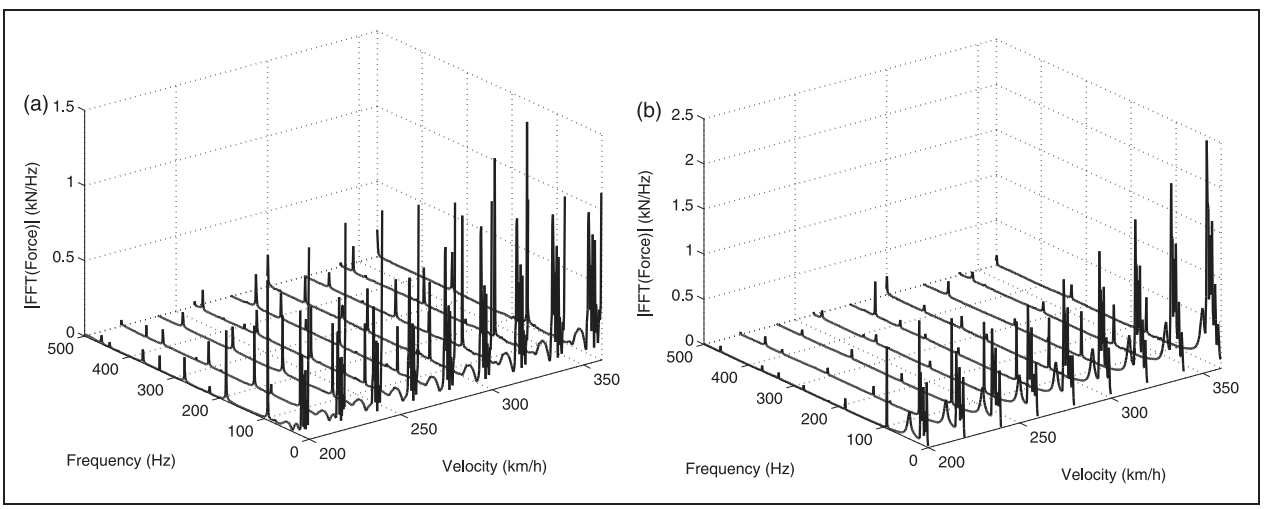

Figure 13. Frequency content of contact force for all velocity with D13's irregularity profile: (a) 2D model; (b) 3D model.

these differences, the qualitative behaviour of both models is similar.

Figure 14 shows the forces transmitted to some railpads during the passage of the vehicle travelling along the track at speed $v = 300$ km/h. The static force obtained in the railpad when the axle load (84.86 kN) is applied on the sleeper is used to compare with the dynamic results.

The vertical acceleration of the rail is represented in Figures 15 and 16 for different speeds of the vehicle. It is obvious that the magnitude of the acceleration of the rail is very sensitive to the vehicle speed: from 167 m/s^2 for $v = 200$ km/h to 306 m/s^2 for $v = 360$ km/h in the 2D analysis, from 117 m/s^2 for $v = 200$ km/h to 314 m/s^2 for $v = 360$ km/h. Comparing Figure 15a with Figure 15b, it can be concluded that in the frequency content, the results obtained in the 2D model and 3D model are similar: both models have peaks at a similar frequency. Furthermore, it can be observed that in the range of frequencies studied ([0–500 Hz]), the lower frequencies has an important influence on the response of both models.

To interpret the results adequately and in dimensionless form, the dynamic impact due to the passing vehicle can be evaluated by using the concept of the dynamic amplification factor

$$\varphi = \frac{F_{dyn}}{F_{sta}} \tag{16}$$

where F_{sta} is the static response and F_{dyn} is the maximum dynamic response obtained in the simulation. Figures 17 and 18 illustrate the dynamic amplification factors, respectively, for the wheel–rail

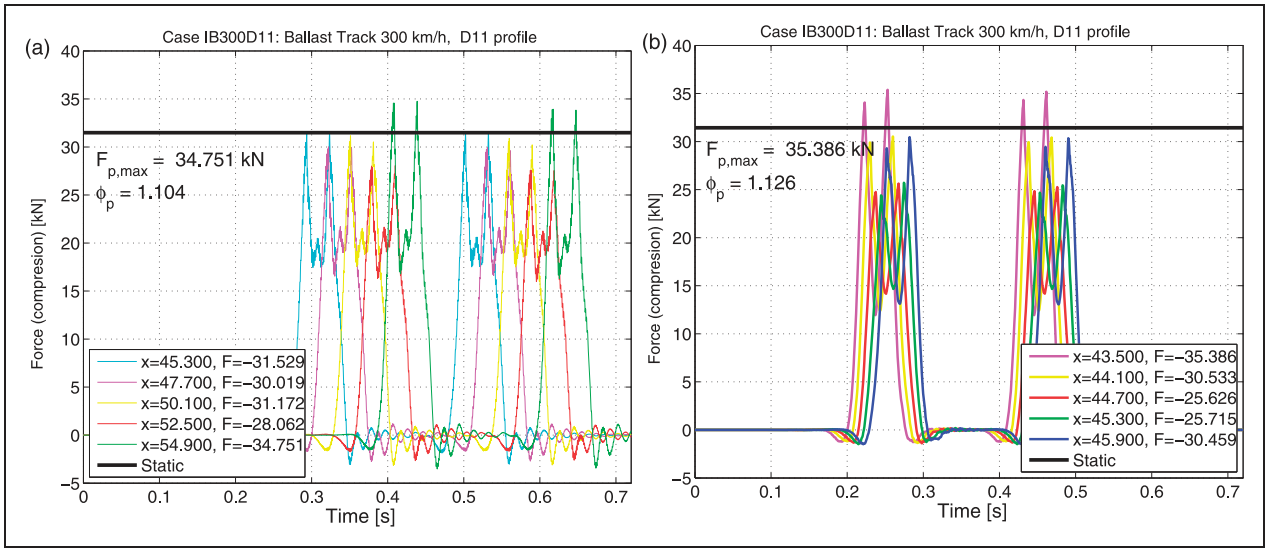

Figure 14. Force transmitted in railpads: (a) 2D model result and (b) 3D model result.

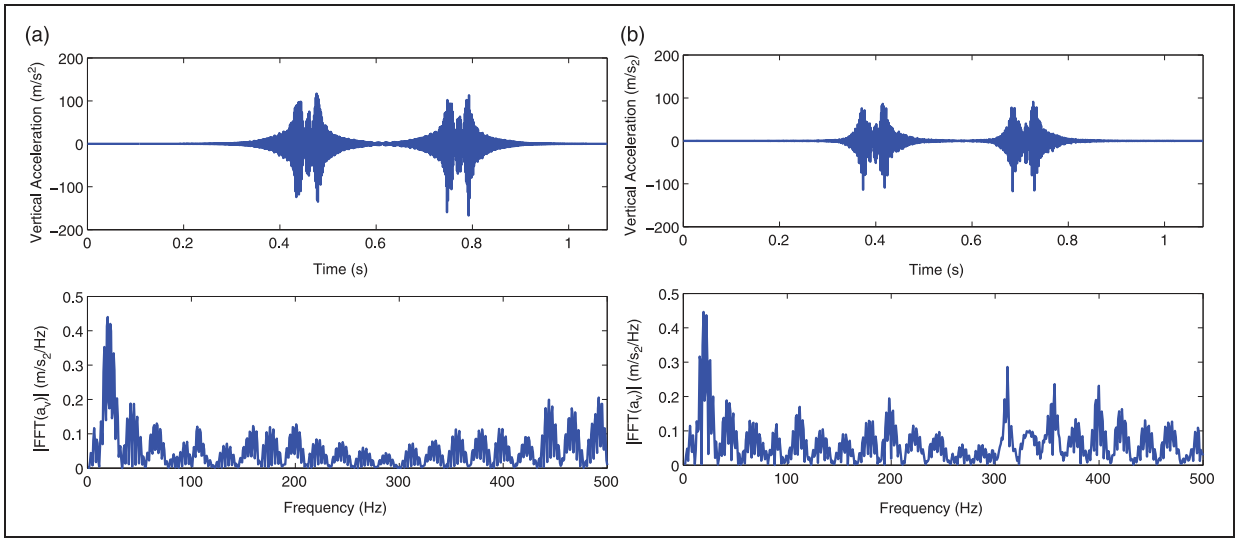

Figure 15. Time history and frequency content of vertical acceleration of the rail during the passage of vehicle on track at speed $v = 200$ km/h with D13 profile: (a) 2D model results; (b) 3D model results.

contact force and the forces transmitted to the railpads for each irregularity profile as a function of train speed, showing also an envelope for the different profiles. It is noted that the irregularities of the track and the train speeds have a strong influence on the dynamic responses of railway track structures induced by traffic loads. In general, the amplification factor increases with speed. However, this is not always the case, and in some situations, critical velocities may be obtained.

Comparison between 2D and 3D results

Some representative results for both 2D and 3D simulations have been shown in Figures 11–18 in the previous subsection on simulation results. The results of the 2D analysis are compared with the corresponding 3D results, and the following general remarks are made.

- Differences between the dynamic response of the two models proposed are small. These differences are most apparent in the amplitude of response. In the frequency content of the contact force (see Figure 13), there is a difference in the frequency of the maximum amplitude: in the 2D model, the sleeper passage frequency has a notable influence, whereas in the 3D model, the frequency of the irregularities has more effects.
- The computational time consumed in the 2D model is relatively small (approximately 6 minutes per simulation), whereas the computational cost of the 3D simulation is very high (using a computer with six processors, the simulation time is 8

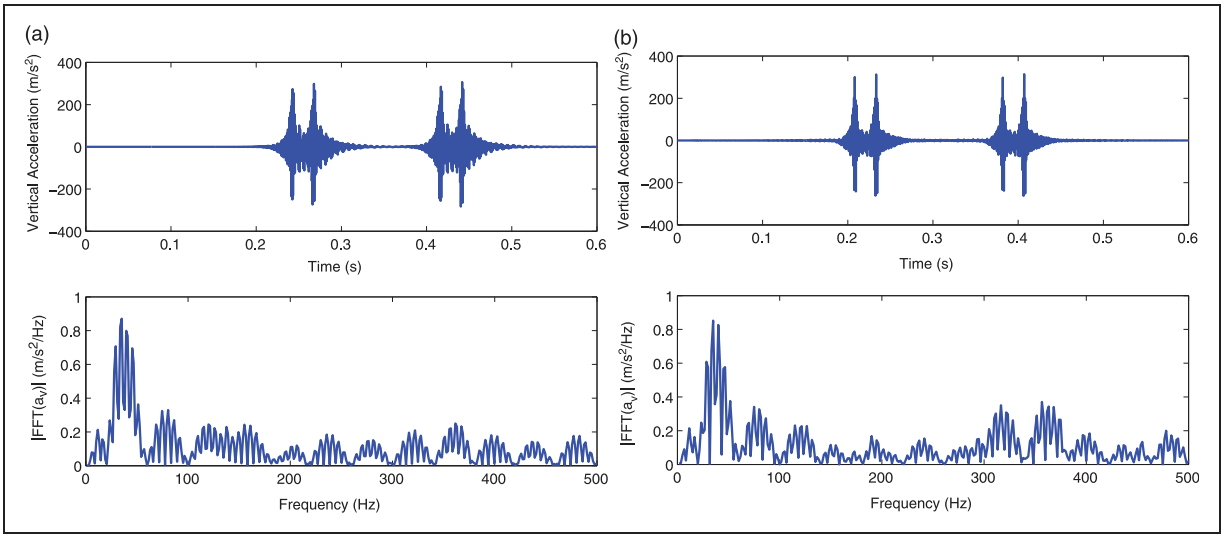

Figure 16. Time history and frequency content of vertical acceleration of the rail during the passage of vehicle on track at speed $v = 360$ km/h with D13 profile: (a) 2D model results; (b) 3D model results.

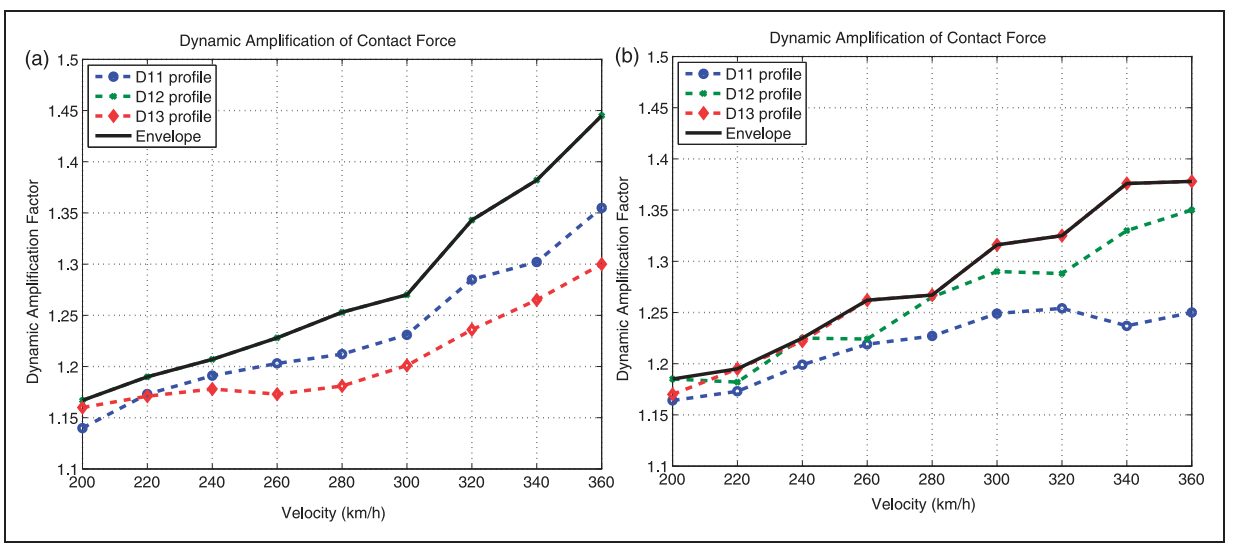

Figure 17. Envelope of dynamic amplification factor of wheel–rail contact force: (a) 2D model results; (b) 3D model results.

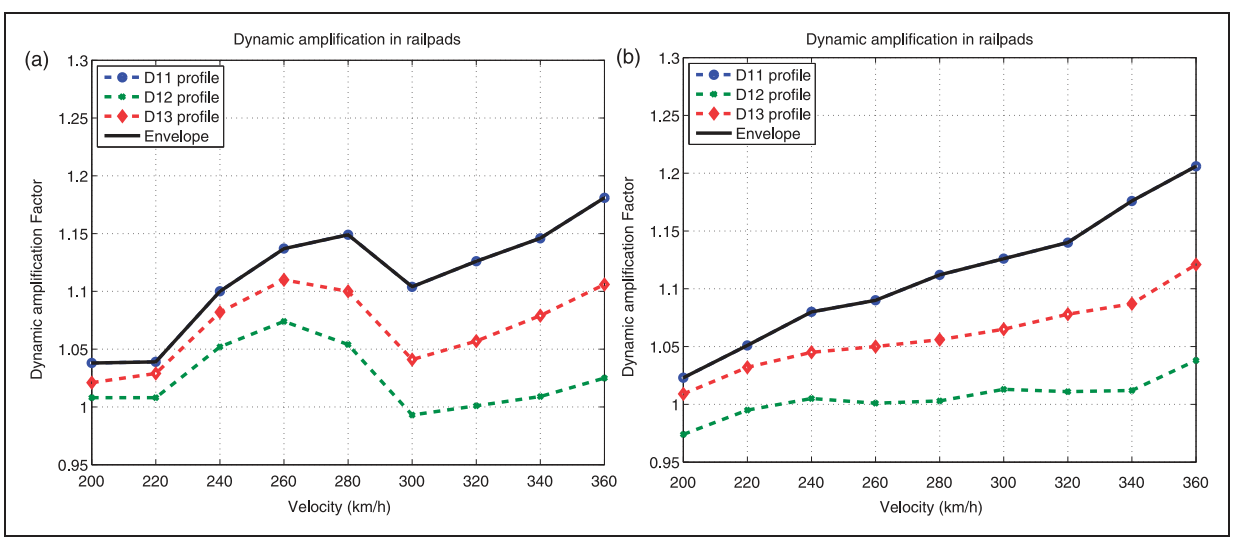

Figure 18. Envelope of dynamic amplification factor of forces transmitted to railpads: (a) 2D model results; (b) 3D model results.

hours). Therefore, the 3D model is costly, not practical from a computational point of view.
- The dynamic impact factor obtained with both analyses is very similar, demonstrating that the 2D model is capable of predicting the main features of the vertical dynamic response for both the vehicle and railway track components (see Figures 17 and 18).

Conclusions

- The dynamic effects of the high-speed traffic load on ballasted track have been studied using two interaction models. The first one is the simplified 2D finite-element model, which neglects the lateral effects and considers a discrete model for ballast and subgrade. The second is a full 3D finite-element model with continuum elements for the ballast and subgrade and infinite elements in the boundary.
- Several vertical track irregularity profiles are generated from PSD and are included in the vehicle–track interaction. The nonlinear Hertz spring is considered for the wheel–rail contact, and the Lagrange multiplier method is used for the contact constraint enforcement. Analysing the results obtained in the interaction of both models, it is noted that the dynamic effects of high-speed traffic loads on the ballast tracks are sensitive both to the track irregularities and the vehicle speed.
- The dynamic response of the vehicle running on the track structure with irregularity profiles is predominantly due to the vibration of the bogie at a lower frequency than the fundamental frequencies of the track structure.
- Comparing the results of the 2D model with the 3D model, it has been found that although there is an unavoidable difference of the dynamic response between track models, there are similar levels of dynamic increments. Therefore, the 2D model can predict the vertical dynamic response with sufficient accuracy.
- On the basis of this study, it may be concluded that the 2D vehicle–track model can be employed for a quick and sufficiently accurate assessment of predicting the dynamic responses of the vehicle and the rail track components. The 2D model is also capable of examining the influence of the properties of the rail track and the vehicle components on the contact force and other dynamic responses of the rail track system.

Funding

This work was supported by the 'Ministerio de Ciencia e Innovación' of the Spain Government through subprogram INNPACTO and project VIADINTEGRA [ref. IPT-370000-2010-012]. The authors are also grateful for the support provided by the Technical University of Madrid, Spain. K. Nguyen would like to express gratitude to AECID for a PhD grant during this study.

References

1. European Committee for Standardization, European Union. *EN 1991–2:2003, Eurocode 1: actions on structures part 2: traffic loads on bridges*. CEN, Brussels, 2003.
2. European Committee for Standardization, European Union. *EN 1990:2002/A1:2005–Eurocode–basis of structural design. Annex A2. Application for bridges*. CEN, Brussels, 2005.
3. European Railway Agency, European Union. *Technical specification for interoperability relating to the infrastructure sub-system of the trans-European high-speed rail system*. ERA, 2007.
4. Knothe K and Grassie SL. Modelling of railway track and vehicle/track interaction at high frequencies. *Veh Syst Dyn* 1993; 22(3-4): 209–262.
5. Dahlberg T. Vertical dynamic train/track interaction – verifying a theoretical model by full-scale experiments. *Veh Syst Dyn* 1995; 24(1): 45–57.
6. Cai Z and Raymond GP. Modelling the dynamic response of railway track to wheel/rail impact loading. *Struct Eng Mech* 1994; 2: 95–112.
7. Zhai W and Cai Z. Dynamic interaction between a lumped mass vehicle and a discretely supported continuous rail track. *Comp Struct* 1997; 63: 987–997.
8. Sun YQ and Dhanasekar M. A dyanmic model for the interaction of the rail track and wagon system. *Int J Solids Struct* 2002; 39: 1337–1359.
9. Esveld C. *Modern railway track*. *MRT Productions* 2001.
10. Lei X and Noda NA. Analyses of dynamic response of vehicle and track coupling system with random irregularity of track vertical profile. *J Sound Vib* 2002; 258: 147–165.
11. Lou P and Zeng QY. Vertical vehicle track coupling element. *Proc IMechE, Part F: J Rail and Rapid Transit* 2006; 220(3): 293–304.
12. Yang SC. Enhancement of the finite-element method for the analysis of vertical train-track interactions. *Proc IMechE, Part F: J Rail and Rapid Transit* 2009; 223(6): 609–620.
13. Popp K, Kaiser I and Kruse H. System dynamics of railway vehicles and track. *Archive Appl Mech* 2003; 72: 949–961.
14. Sun YQ, Dhanasekar M and Roach D. A three dimensional model for the lateral and vertical dynamics of wagon track systems. *Proc IMechE, Part F: J Rail and Rapid Transit* 2003; 217(1): 31–45.
15. Kumaran G, Menon D and Nair KK. Dynamic studies of railways sleepers in a track structure system. *J Sound Vib* 2003; 286: 485–501.
16. Lundqvist A and Dahlberg T. Load impact on railway track due to unsupported sleepers. *Proc IMechE, Part F: J Rail and Rapid Transit* 2005; 219: 67–77.
17. Sun YQ and Simson S. Nonlinear three dimensional wagon track model for the investigation of rail corrugation initiation on curved track. *Veh Syst Dyn* 2007; 45(2): 113–132.

18. Zhai W, Wang K and Cai C. Fundamentals of vehicle track coupled dynamics. *Veh Syst Dyn* 2009; 47(11): 1349–1376.
19. Dahlberg T. Railway track stiffness variations consequences and countermeasures. *Int J Civil Eng* 2010; 8(1): 1–12.
20. Dassalt Systemes SIMUIA Corp. *ABAQUS analysis user's manualv*, *6.11*. Dassalt Systemes SIMULIA Corp., 2011.
21. Ishida M and Suzuki T. Effect on track settlement of interaction exited by leading and trialing axles. *QR of RTRI* 2005; 46(1).
22. Knothe K and Wu Y. Receptance behaviour of railway track and subgrade. *Archive Appl Mech* 1998; 68: 457–470.
23. Melis M. Embankments and ballast in high speed rail. Fourth part: high-speed railway alignments in Spain. Certain alternatives. *Revista Obras Públicas* 2007; 3476: 41–66.
24. Zhai WM, Wang KY and Lin JH. Modelling and experiment of railway ballast vibrations. *J Sound Vib* 2004; 270(4–5): 673–683.
25. Costa PMBA. *Vibrações do sistema via-maciço induzidas por tráfego ferroviário. Modelação numérica e validação experimental*. Porto: Universidade do Porto, 2011.
26. Chopra AK. *Dynamics of structures: theory and applications to earthquake engineering*. 2nd ed. Prentice Hall, 2000.
27. Ma L, Liu W, Zhang H, et al. Influence of track parameters on rail frequency response function based on analytical solution. In: *Advances in environmental vibration – proceedings of the fifth international symposium on environmental vibration*. Science Press, 2011, pp.700–706.
28. Clauss H and Schiehlen W. Modeling and simulation of railways bogie structural vibrations. *Veh Syst Dyn* 1998; 29(1): 538–552.
29. European Committee for Standardization, European Union. *EN 13848-5:2008 railway applications–track–track geometry quality part5:geometric quality levels*. CEN, Brussels, 2008.
30. Johnson KL. *Contact mechanics*. Cambridge: Cambridge University Press, 1985.
31. Ministerio de Fomento de España. "Instrucción de acciones a considerar en el proyecto de puentes de ferrocarril (IAPF)". *Dirección General de Ferrocarriles*, Madrid, 2007.

Appendix 1: Properties of models

Table 3. Main parameters of railway vehicle and track used in the simulation.

Notation	Parameter	Value
Vehicle system		
L_b	Distance between bogies (m)	17.375
L_a	Distance between wheelsets in bogie (m)	2.5
$M_c = 8m_c$	Mass of car body (kg)	53,500
J_{cx}	Mass moment of inertia of car body about X axis (kg m^2)	9.57×10^4
J_{cy}	Mass moment of inertia of car body about Y axis (kg m^2)	1.69×10^6
J_{cz}	Mass moment of inertia of car body about Z axis (kg m^2)	1.69×10^6
$M_b = 4m_b$	Mass of bogie (kg)	3500
J_{bx}	Mass moment of inertia of bogie about X axis (kg m^2)	2231
J_{by}	Mass moment of inertia of bogie about Y axis (kg m^2)	4569
J_{bz}	Mass moment of inertia of bogie about Z axis (kg m^2)	2802
$M_w = 2m_r$	Mass of wheelset (kg)	1800
J_{wx}	Mass moment of inertia of wheelset about X axis (kg m^2)	880
k_{2v}	Stiffness coefficient of secondary suspension along Y axis (kN/m)	410
c_{2v}	Damping coefficient of secondary suspension along Y axis (kN s/m)	45
k_{2h}	Stiffness coefficient of secondary suspension along Z axis (kN(m)	315.6
c_{2h}	Damping coefficient of secondary suspension along Z axis (kN s/m)	50
k_{2l}	Stiffness coefficient of secondary suspension along X axis (kN(m)	500
c_{2l}	Damping coefficient of secondary suspension along X axis (kN s/m)	65.4
k_{1v}	Stiffness coefficient of primary suspension along Y axis (kN/m)	873
c_{1v}	Damping coefficient of primary suspension along Y axis (kN s/m)	24
k_{1h}	Stiffness coefficient of primary suspension along Z axis (kN/m)	5100
c_{1h}	Damping coefficient of primary suspension along Z axis (kN s/m)	58.86
k_{1l}	Stiffness coefficient of primary suspension along X axis (kN/m)	24,000
c_{1l}	Damping coefficient of primary suspension along X axis (kN s/m)	19.62

(continued)

Table 3. Continued

Notation	Parameter	Value
Track system		
L	Model length (m)	90.0
h_b	Ballast thickness (m)	0.40
l_s	Sleeper spacing[a] (m)	0.60
	Rail	UIC60
k_p	Railpad stiffness[b] (MN/m)	100
c_p	Railpad damping[a] (MN s/m)	0.015
k_b	Ballast stiffness[b] (MN/m)	100
c_b	Ballast damping[c] (MN s/m)	0.0253
k_c	Subgrade stiffness (MN/m)	80
c_c	Subgrade damping[c] (MN s/m)	0.0455
m_t	Half sleeper mass[a] (kg)	160
m_{ba}	Ballast mass (kg)	646
E_b	Elastic modulus of ballast (MN/m^2)	68.44
E_f	Elastic modulus of subgrade (MN/m^2)	90
E_s	Elastic modulus of sleeper[c] (MN/m^2)	38.45×10^3
ρ_b	Ballast density[a] (kg/m^3)	1800
ρ_f	Subgrade density[a] (kg/m^3)	1800
ρ_s	Sleeper density[a] (kg/m^3)	2400
l_b	Sleeper width underside[a] (m)	0.3
l_e	Effective supporting length of half sleeper[a] (m)	0.95
ϕ_b	Ballast stress distribution angle[a]	35°

[a]Assumed value.[15,18,24,31]

[b]The values taken from the data of AVE Zaragoza track.

[c]The value is calculated based on the proposition of the damping coefficients of ballast and subgrade as 10% of their critical damping coefficients. The elastic modulus of ballast E_b is calculated by equation (6).